Scientific Research Publishing

Open Journal of Fluid Dynamics, 2016, 6, 438-452
http://www.scirp.org/journal/ojfd
ISSN Online: 2165-3860
ISSN Print: 2165-3852

Study on the Shear Effect on Dye Patches Diffused in Wall-Bounded Shear Flow

Qianqian Shao, Takahiro Tsukahara, Yasuo Kawaguchi

Department of Mechanical Engineering, Tokyo University of Science, Chiba, Japan
Email: sqq1990dd@163.com, tsuka@rs.tus.ac.jp, yasuo@rs.noda.tus.ac.jp

How to cite this paper: Shao, Q.Q., Tsukahara, T. and Kawaguchi, Y. (2016) Study on the Shear Effect on Dye Patches Diffused in Wall-Bounded Shear Flow. *Open Journal of Fluid Dynamics*, **6**, 438-452.
http://dx.doi.org/10.4236/ojfd.2016.64032

Received: October 19, 2016
Accepted: December 26, 2016
Published: December 29, 2016

Abstract

This paper focuses on the high intensity filaments (dye patches) embedded in dye plumes in a wall-bounded shear flow, to investigate the shear effect on the dye patch distribution. Motivated by the widely concerned inverse estimation of the source location, we try extracting useful information to know the source location from downstream dye patches. Accordingly, we changed the dye injection location at different distances from the wall and made observations at different downstream (diffusion) distances from the source. The orientation angle and roundness of dye patches were concerned to examine the shear effect and dye patch characteristics. To capture the dye plume images, a planar laser induced fluorescence (PLIF) technique was used. The orientation and roundness of each dye patch were calculated by least-square fitting. The statistics of both the orientation angle and the roundness were compared with those in homogeneous turbulent cases to reveal the shear effect. Different from uniformly-orientated dye patches in the homogeneous flow, larger occurrence probabilities with positive orientation angles of dye patches are observed in wall-bounded shear flow, in particular, when the injection location is near the wall. As with information extraction for the inverse estimation of source location, it is found that the orientation distribution of dye patches is independent of the diffusion distance, but related with the injection location from the wall. While for the homogeneous flow cases, a strong dependence on the diffusion distance is observed in the orientation distribution profiles. As for the roundness, similar aspects are found regarding the dependencies on the injection location in shear flow and on diffusion distance in homogeneous flow.

Keywords

Dye Patch, Image Processing, Inverse Problem, Least-Square Fitting, Passive Scalar, Shear Flow, Source Estimation, Point-Source Diffusion, Wall Turbulence

1. Introduction

From the viewpoint of protecting environment, the problem of pollutant dispersion has

always been put considerable attention. Dispersion of passive contamination injected into a turbulent flow has been studied mostly, on one hand due to its simplicity without buoyancy effects or sedimentation, on the other hand because of the universality of turbulent flow in nature or engineering problem. Such research can be as previous as G. I. Taylor, who did a foundation research concerning the random motion of an individual fluid particle released from a fixed point in homogeneous isotropic turbulence [1]; followed by Richardson, who developed the theory on relative dispersion in turbulent flows [2]. Recently, by virtue of advanced scalar field measurement technique, researches are largely carried out to investigate the characteristics of turbulent diffusion [3] [4] [5]. Based on the better understanding of the characteristics of turbulent diffusion field, one application is the inverse estimation of the pollutant release location. Webster *et al*. [6] inspired by food or mate locating of animals, proposed a bilateral comparison method for tracking turbulent chemical plume source, besides, the integral spanwise length scale was also indicated to be suitable for source localization. Tsukahara *et al*. [7] used the time-averaged concentration and root mean square of concentration fluctuations to conduct inverse source localization of dye release based on the Taylor's diffusion theory. Their source-locating method was tested in the framework of a water channel-flow experiment providing a rather homogeneous turbulent field in the channel central region. Besides the statistical characteristics of the plume, the high intensity areas in the plume also contain much information for inverse estimation of the plume release source location [8] [9] [10] [11]. For example, Moore and Atema [8] concerned the characteristic of dye pulses including the distribution of the mean pulse height, pulse onset slope, probability of above-average pulse height, and indicated that these features would be useful as directional cues for source localization. Webster and Weissburg [9] found the time-averaged value of the rise slope to vary systematically with diffusion distance.

Different from the dye dispersion in homogeneous flow, dye released into the wall-bounded shear flow suffers strong shear and stretching. Crimaldi *et al*. [12] studied the instantaneous and statistical plume characteristics using experiment method by releasing dye solution on ground level into a turbulent flow. From the instantaneous dye plume images, stretched and strained filaments were observed. In [13], the shear effect on the dispersion of passive contamination in turbulent flow was concerned by injecting the plume from two different heights (one is a ground-level source, the other is an elevated source). By comparison of the concentration field, the effects of the plume source size and wall-normal height were discussed. Based on this research, the maximum mean concentration and the lateral plume width in the shear flow were found to be related with the downstream distance.

According to these relevant works, this paper focuses on the dye patches of passive scalar diffusion in a wall-bounded shear flow, aims to study the shear effect on dye patch distribution, and try to extract useful information for inverse source location estimation. For this purpose, we consider a single-source dispersion where dye solution is injected into a wall-bounded turbulent shear flow in a water channel. Four dye injection

locations at different wall-normal distances are selected (similar with the source height in [13]), while six downstream observation sites are set located at different downstream distances from the release source. For each combination of the four injection locations and six diffusion distances, a time series of dye plume images are taken with a planar laser induced fluorescence (PLIF) technique. The shear effect analysis and information extraction for inverse source-location estimation are to be performed through image processing, calculating the orientation and roundness of each dye patch, and making statistical analysis.

In Section 2, our experimental apparatus is shown with the experimental conditions; in Section 3, the procedures of image processing are given, by which dye patches are extracted from the dye plume; in Section 4, the least-square fitting method to calculate the orientation and roundness of dye patches is introduced; in Section 5, the results are analyzed to show the shear effect on dye patch distribution and to extract information available for the source estimation; and Section 6 is the final conclusion.

2. Experiment

2.1. Experimental Setup

Figure 1 shows the setup of the experiment, with Figure 1(a) being the sketch of the water loop and Figure 1(b) being the sketch of the measurement section. In both figures, x defines the streamwise direction; z defines the spanwise direction; y defines the direction perpendicular to x and z directions. As this research concerns dye dispersion in wall-bounded shear flow, a channel flow and dye injection into the flow is simulated, and the dye plume is recorded by a two-dimensional PLIF technique. In Figure 1(a), water in the tank is pumped into the pipe, enters the rectangular channel after passing a honeycomb, and then returns to the tank. The rectangular channel is made of plexiglass to ensure optical access, with a 500 mm width (l_z) and a 40 mm between-side-wall distance (l_y). The measurement section locates at the downstream part of the rectangular channel, which is far downstream from the channel entry to assume a fully-developed turbulent flow in the measurement section. The PLIF technique is used to capture the dye dispersion plume at the designated observation sites. At the measurement section, there are laser-access and observation windows (not shown in Figure 1). As the PLIF images are taken on the xy plane at the height of the laser access window, the imaged flow is a wall-bounded shear flow and z direction is not considered here.

2.2. Experimental Condition

Rhodamine-WT is used as the dye, and the injection of dye solution is isokinetic with the local flow and assumed to be passive in the flow field. As is shown in Figure 1(b), the height of dye release source is along the horizontal centerlines of the laser access windows. The fluid temperature is kept at 25˚C by the heater. The Reynolds number in is $Re = l_y U_B / \nu = 20{,}000$, with U_B being the bulk velocity of the flow in the measurement section, and ν being the kinematic viscosity of water.

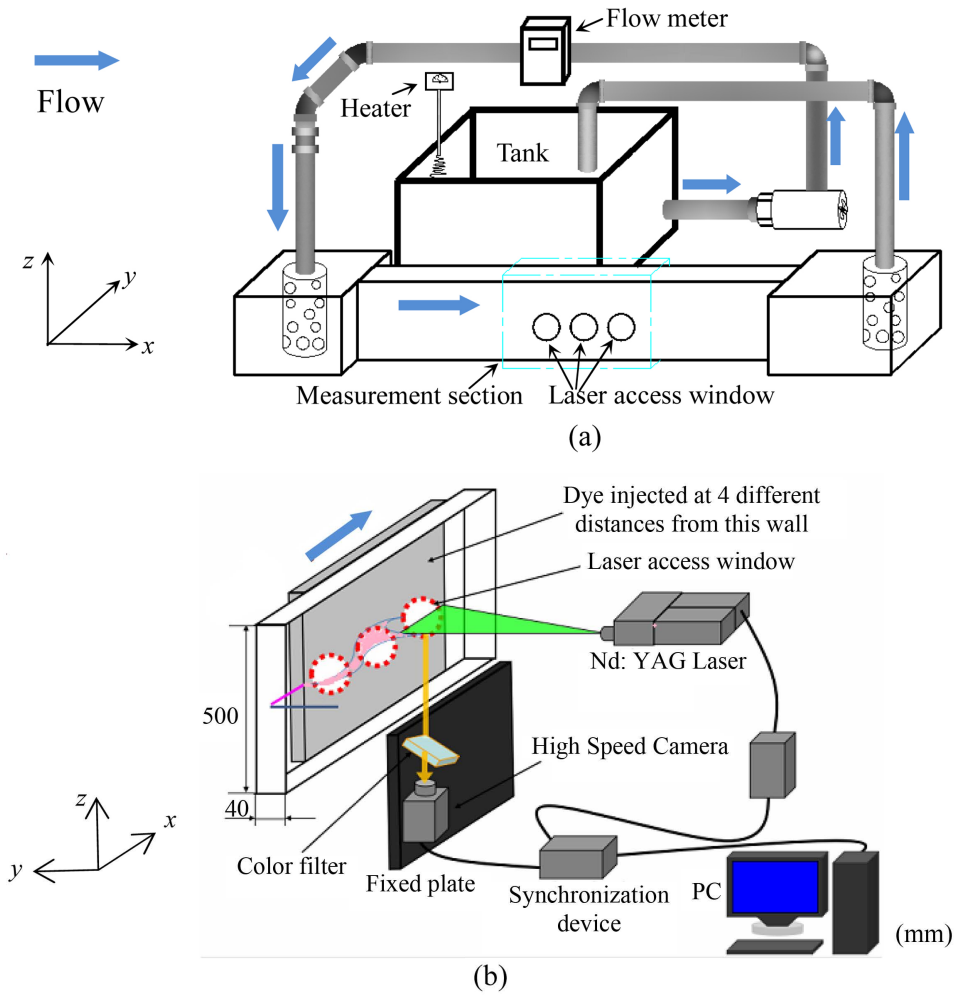

Figure 1. Schematic diagram of the experiment apparatus of PLIF measurement. (a) Experimental water loop; (b) Measurement section.

Four injection locations are selected at $Y^* = Y/l_y = 0$, 1/8, 1/4, and 1/2, with Y being the wall-normal distance between the injection source and the reference wall. The six normalized diffusion distances are $X^* = 4X/l_y = 20$, 30, 45, 50, 90, and 100, with X being the diffusion distance, that is, the streamwise distance between the downstream observation sites and the release source. For each combination of the injection location and diffusion distance, a time series of 500 dye-plume images are obtained through the PLIF measurement.

3. Image Processing for Dye Patch Extraction

Through PLIF measurement, a time series of dye plume images are obtained. Examples of the PLIF images are shown in **Figure 2(a)**.

The domain is 40 × 40 mm^2, cut from the 2048 × 2048 pixels to be convenient for analysis. Here, it is worth to note the images for the two samples share the same x and y

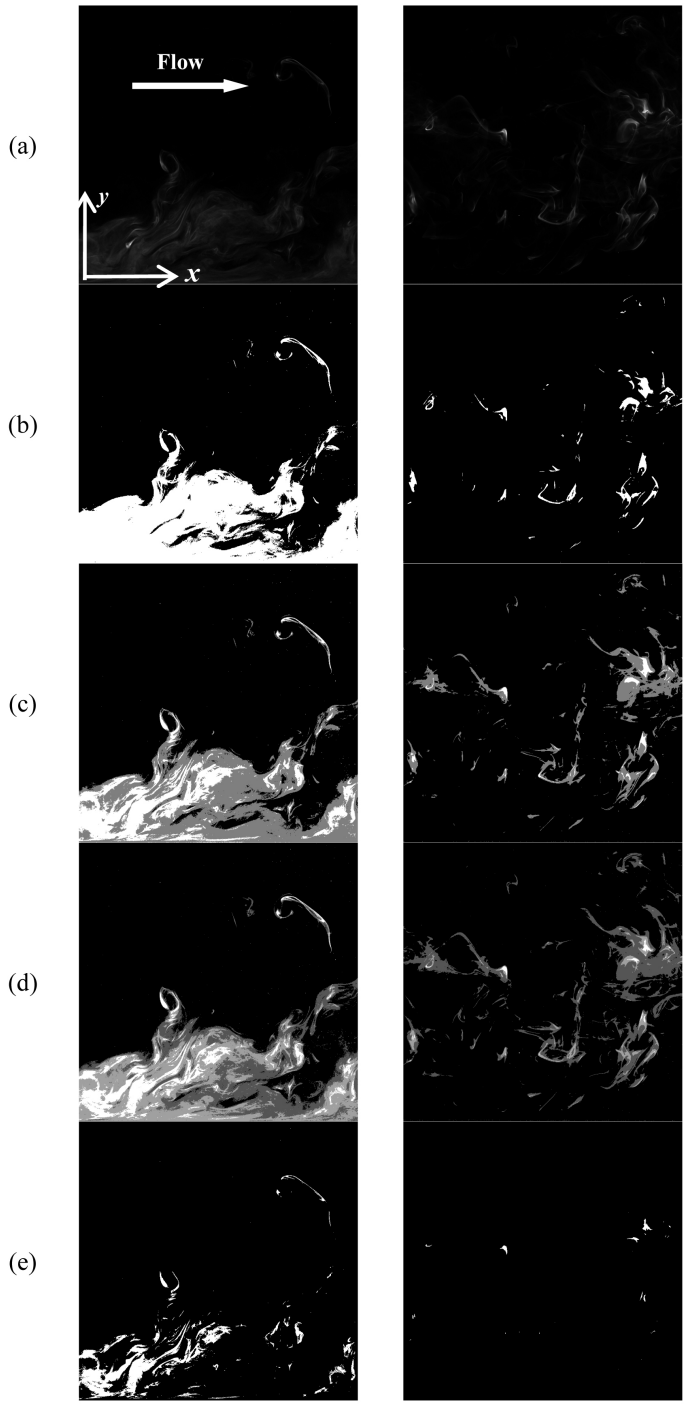

Figure 2. Examples of multilevel thresholding of PLIF images for two sampling conditions: $X^* = 30$ and $Y^* = 0$, and $X^* = 30$ and $Y^* = 1/2$. (a) Raw images of dye plume, (b) binarized images by "regular" binarization based on threshold by Otsu's method, (c) the three-level images, (d) the four-level images, and (e) the binarized images by "irregular" binarization based on the third level threshold of four-level image obtained by multilevel thresholding.

coordinate directions, however, with the coordinate origin being the respective left bottom point of the analyzed image. From raw images, randomly distributed high-intensity areas can be seen in the plume. To extract these filaments from the plume, bi-level thresholding and connected-component labeling are performed.

3.1. Bi-Level Thresholding

Figures 2(b)-(e) show the different thresholding results of **Figure 2(a)**, with the left column being the images for $X^* = 30$ and $Y^* = 0$, while the right column being the images for $X^* = 30$ and $Y^* = 1/2$. Mostly, the binarization threshold is determined by Otsu's method [14], and the binarization based on this threshold is called regular binarization here. **Figure 2(b)** provides the results by regular binarization. The white areas in **Figure 2(b)** are concerned to be dye patches, while black areas mean no dye patch there. Comparing between **Figure 2(a)** and **Figure 2(b)**, large difference exists, although the white areas can mark the high-intensity filaments in **Figure 2(a)**. The solution is to improve and at the same time automatically determine the threshold. We resort to the highest threshold in multilevel thresholding [15], similarly with Otsu's method, determining the thresholds by maximizing the between-class variance σ_B^2 as,

$$\begin{aligned} &\sigma_B^2 = \sum_{k=1}^{M} \omega_k \left(\mu_k - \mu_t\right)^2 \\ &\omega_k = \sum_{i=i_{th,k-1}+1}^{i_{th,k}} P_i,\ \mu_k = \sum_{i=i_{th,k-1}+1}^{i_{th,k}} \left[\frac{iP_i}{\omega_k}\right],\ \mu_t = \sum_{k=1}^{M} \omega_k \mu_k, \end{aligned} \tag{1}$$

where M is the aimed number of gray intervals reduced from the original 256 gray levels, $(M-1)$ thresholds are to be determined to separate the pixels at the original 256 gray levels into the aimed M gray intervals, and these $(M-1)$ thresholds are represented as $i_{th,1}, i_{th,2}, \cdots, i_{th,(M-1)}$. In Equation (1), P_i is the probability of the pixels with gray level i, while k is the k-th gray level interval.

Based on the multi-level thresholds calculated this way, examples of three-level images and four-level images are given in **Figure 2(c)** and **Figure 2(d)**, where different gray levels denote different brightness intervals. It can be seen that the highest level shown in **Figure 2(d)** match the high concentration filaments well, and also the computer time consumed is acceptable. Then, we conducted the binarization based on the highest threshold of the four-level images, and the binarization result is given as **Figure 2(e)**, which we call irregular binarization. In this research, the following analysis has been based on the binarized images obtained this way.

3.2. Connected Components Labeling

After the dye patches in the images are highlighted, they are separated and numbered by connected components labeling [16], as **Figure 3** shows. The highlighted areas on the bi-level image is labeled into different dye patches according to the connectivity and one gray level denotes one independent high-intensity dye patch, while the gray levels on the labeled images are not related with the original gray levels in the dye patch. To

(a) Bi-level image (b) After labeling

Figure 3. Example of connected components labeling. In (a), the white areas is dye patches; in (b), the dye patches in (a) are separated apart by assigning different gray levels.

avoid noises, dye patches with small number of pixels are ignored and only those containing more than 8 pixels are taken into consideration for later analysis.

4. Orientation and Roundness

To see the shear effect on the dye patches, we consider to use orientation and roundness. The orientation angle and roundness of each dye patch are calculated based on the following procedures. **Figure 4** is a schematic sketch of a dye patch. The angle α ($\alpha = \theta - 90^\circ$) is the defined orientation angle of this patch. To be convenient, the orientation angle is required to be within the range (–90˚, 90˚). The coordinate is the corresponding coordinate for the analyzed images taken at different observation sites.

To calculate α, least square fitting method is used, by minimizing the sum of the squared perpendicular distances d_{ij} of all the pixels in this patch from the fitting line. Considering that the filaments extracted have small within variance, the difference of original concentrations of the pixels in one filament can be neglected and treated as the same value. Assuming that the region containing the dye patch has M pixels in x direction, and N pixels in y direction, the sum which is to be minimized in least square fitting is,

$$\chi^2 = \sum_{i=1}^{M}\sum_{j=1}^{N} d_{ij}^2 G[i, j] \tag{2}$$

In Equation (2), $G[i, j] = B[i, j]$ that is 1 in the dye patch, 0 outside the dye patch. d_{ij}^2 is the squared perpendicular distance of pixel (i, j) in the patch from the fitting line. The line is expressed in polar coordinate as $\rho = x\cos\theta + y\sin\theta$ and the distance can be expressed as $d_{ij}^2 = \left(x_{ij}\cos\theta + y_{ij}\sin\theta - \rho\right)^2$.

Minimizing is achieved by $\partial\chi^2 / \partial\theta = 0$, and yields,

$$\rho = \overline{x_z}\cos\theta + \overline{y_z}\sin\theta \tag{3}$$

$\left(\overline{x_z}, \overline{y_z}\right)$ is the gravity center of the dye patch. By introducing $x'_{ij} = x_{ij} - \overline{x_z}$, $y'_{ij} = y_{ij} - \overline{y_z}$, we have,

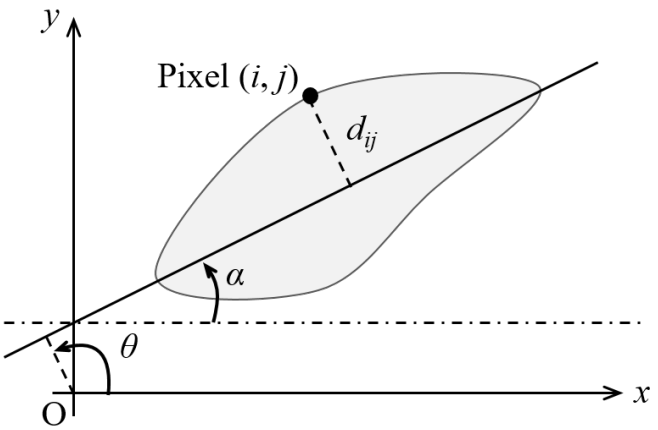

Figure 4. Schematic diagram of a dye patch in wall-bounded shear flow: the line represents the least square fitting line for the shape of this patch.

$$\chi^2 = \sum_{i=1}^{M}\sum_{j=1}^{N}\left\{\left(x'_{ij}\cos\theta + y'_{ij}\sin\theta\right)^2 G[i,j]\right\} \tag{4}$$

Extending and arranging Equation (4) lead to,

$$\chi^2 = a\cos^2\theta + b\cos\theta\sin\theta + c\sin^2\theta \tag{5}$$

The solution satisfies:

$$\sin 2\theta = \pm\frac{b}{\sqrt{b^2+(a-c)^2}} \quad \text{and} \quad \cos 2\theta = \pm\frac{a-c}{\sqrt{b^2+(a-c)^2}}, \text{ with:}$$

$$a = \sum_{i=1}^{M}\sum_{j=1}^{N}\left\{x'^2_{ij}G[i,j]\right\},\ \ b = 2\sum_{i=1}^{M}\sum_{j=1}^{N}\left\{x'_{ij}y'_{ij}G[i,j]\right\}, \text{ and } \ c = \sum_{i=1}^{M}\sum_{j=1}^{N}\left\{y'^2_{ij}G[i,j]\right\}.$$

Then, the orientation angle is calculated by: $\alpha = \theta - 90^\circ$, with unit of [degree]. The roundness by: $E = \chi_{max}/\chi_{min}$, with circle has a roundness of 1 while line has an infinitely large roundness.

5. Results and Discussion

To investigate the statistical characters of the orientation angle and roundness of dye patches, probability distribution function (p.d.f) of α distribution is investigated. For comparison, results for dye injection in homogeneous turbulent flow are firstly given. The related experiment in our group can be seen in [7]. Seven diffusion distances are chosen in the homogeneous case, which are $X^* = 5$, 10, 25, 30, 35, 40, and 60.

Figure 5 shows the orientation angle distribution of high intensity dye patches in the homogeneous flow for seven tested downstream distances. It is seen that, for all tested downstream distances, the p.d.f curves are symmetry against zero degree, with the largest probability occurring at zero degree. Before discussing the result of shear flow, the analysis of the results in the homogeneous flow is necessary, based on which the analysis for shear flow results will be easier. Figure 5 can be explained as the following: firstly, due to the larger integral length scale in the streamwise direction relative to the

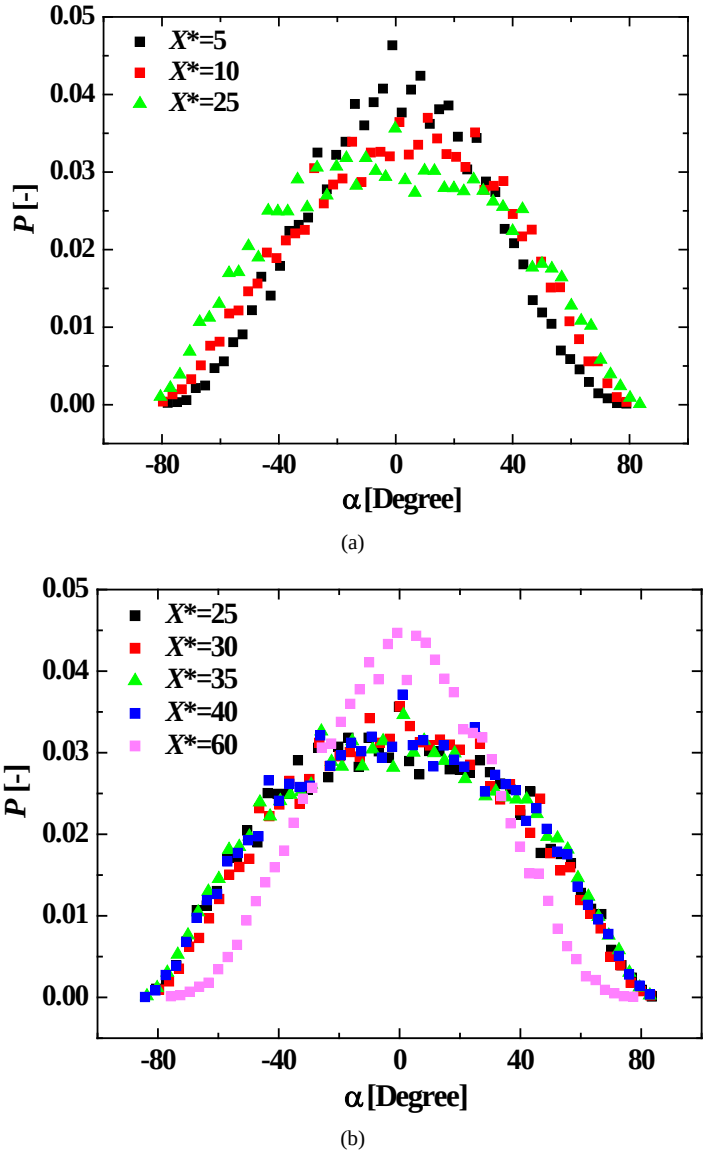

Figure 5. Probability density distribution of the orientation angle (with unit being degree) of dye patches for homogeneous flow, experiment introduced in [7], to see clearly, the results of seven diffusion distances are separated into two sub-figures. (a) X^* = 5, 10 and 25; (b) X^* = 25, 30, 35, 40 and 60.

spanwise direction, dye patches tend to have larger length in the streamwise than in the spanwise direction and thus the calculated orientation angle by the least square fitting method tends to concentrate around zero; secondly, in the homogeneous turbulent flow, the shear effect can be neglected, and the dye patch inclination has equal probability of being positive or negative, that is the high-intensity dye patches distribute randomly in the homogeneous turbulent flow towards positive orientation or negative orientation. To be quantitative, the skewness *Sk* of the orientation angle distribution for all tested downstream distances in the homogeneous case is calculated and given in

Figure 6. The skewness of the distribution of the dye patch orientation angle is around zero, which is consistent with the p.d.f distribution results of the orientation angle and means a symmetry reasonably.

From Figure 5, an obvious diffusion distance-dependence of the p.d.f curve shape is observed, at small X^*, the width of the p.d.f curve increases along with increasing X^*, and the shape tends to be flatter; at large X^*, the width of the p.d.f curve decreases along with increasing X^*, and the shape tends to be sharper. It is inferred that there is a possible turning point, maybe, between $X^* = 25$ to 40. The reason for this tendency is that, when the dye is injected into the flow, it is much connected, and thus the orientation by least square fitting tends to be more around zero or small angle. Towards downstream, it spreads out and the dye patch is much separated and forms spot-like distribution, the orientation angle preference becomes less obvious. While after the turning point, the influence of the side walls cannot be neglected, and the dye spread widely almost across the whole between-wall distances. Dye patch appears to cover a large area, which makes the orientation angle have much larger probability around zero degree. This result also reflects the complexity of the scalar field, and the inverse estimation of source location of the dye release in turbulent flow has many limitations.

Then let us see the results for the wall-bounded shear flow. Due to the number of combination of cases are very large, only representative results are given. Figure 7 is the probability density function distribution of the dye patch orientation for different Y^* at $X^* = 30$. Much different from the homogeneous results, wall-bounded shear flow results show asymmetric distributions of the orientation angle for injection near the wall, for example, $Y^* = 0$ and $Y^* = 1/8$. Towards 1/2, the p.d.f curves tend to be symmetric against zero degree. The asymmetry for small Y^* can be explained as a result of the shear effect in wall-bounded turbulent flow on the dye patches. In the vicinity of the wall, the local mean flow velocity is small; away from the wall, the local mean flow

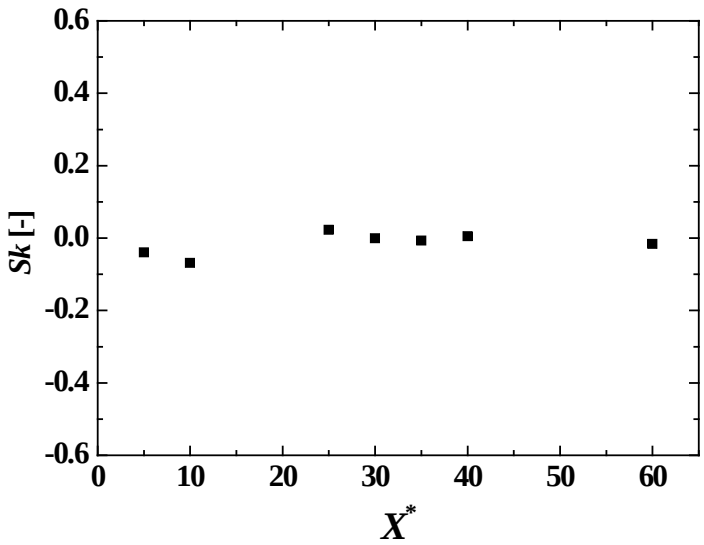

Figure 6. Skewness of orientation angle distribution of dye patches for homogeneous flow.

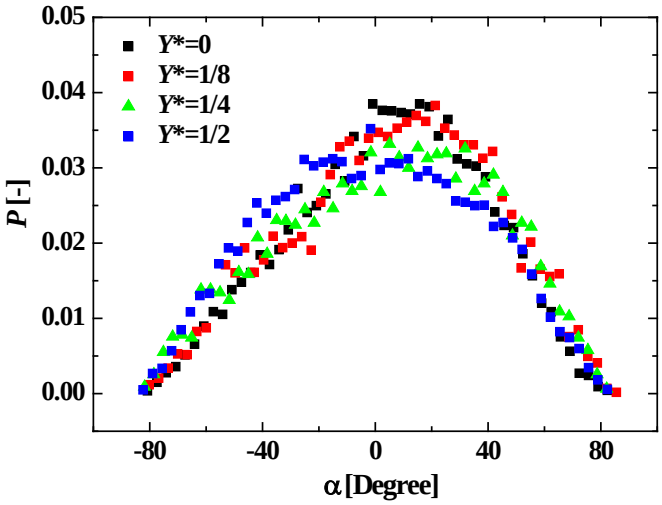

Figure 7. Probability density distribution of orientation angle of dye patches for the case of wall-bounded shear flow: different Y^* for $X^* = 30$.

velocity increases sharply. Such a velocity difference makes the orientation of the dye patches tend positive. Meanwhile, the dominance of the integral length scale in the streamwise direction over spanwise direction is not obvious in the near-wall region. The two effects combine to make positive orientation be dominant for small Y^* in shear flow cases instead of the zero degree in homogeneous cases. While for larger Y^*, for example $Y^* = 1/2$, the orientation angle distribution is nearly symmetric, it can be understood that at the channel center, the shear effect decreases a lot, and the flow can be assumed to be homogeneous flow.

The skewness for the wall-bounded shear flow is given in Figure 8. For most of the cases, the skewness increases with increasing Y^*. This characteristic can be considered due to the affect of the injection location on the shear effect, and the wall-normal distance dependence of the dye patch geometry features can be elucidated. With respect to the streamwise diffusion distance-dependence, Figure 8 provides no hints. Similar with Figure 5, the orientation angle distributions for some X^* are plotted in Figure 9. Unlike the homogeneous cases, where the widths of the p.d.f curves are to some content related with X^*, there is no such phenomenon for the shear flow cases.

As for the roundness for the shear flow and homogeneous flow, see Figure 10 and Figure 11. Comparatively, in the shear flow, the roundness of maximum probability is a little larger than that in the homogeneous flow. As with the shear flow results, it is seen for $Y^* = 0$, the roundness tends to be smaller than $Y^* = 1/8$ or the other two. This is due to the dye-trapping ability of the viscous layer [12]. When injected on the wall, it is easier to find the existence of a persistent, relatively uniform layer of dye within the viscous sublayer, which appears to be connected, larger-area dye patches on the bi-level images. Different from small-area dye patches, large-area dye patches tend to have smaller roundness. As with the homogeneous results, both very near the source and too far away from the source produce higher probability of having smaller roundness. From

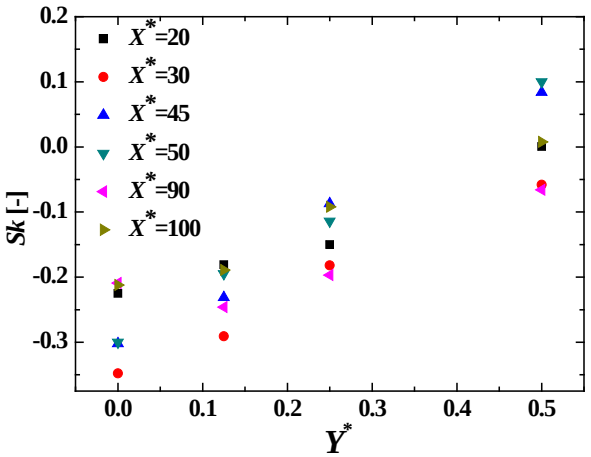

Figure 8. Same as **Figure 6**, but for the wall-bounded shear flow, as a function of Y^*.

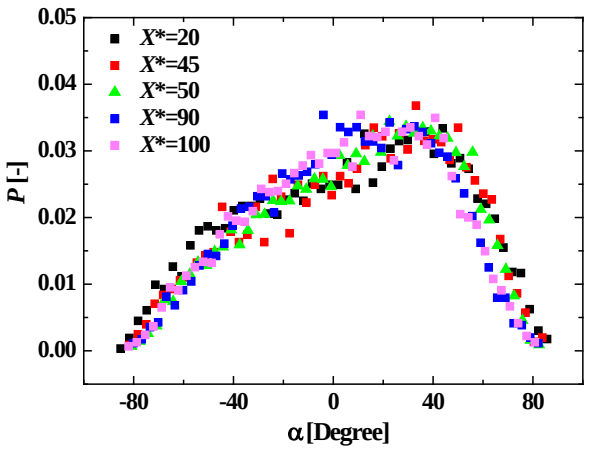

Figure 9. Same as **Figure 7**, but for the wall-bounded shear flow: different X^* for $Y^* = 0$.

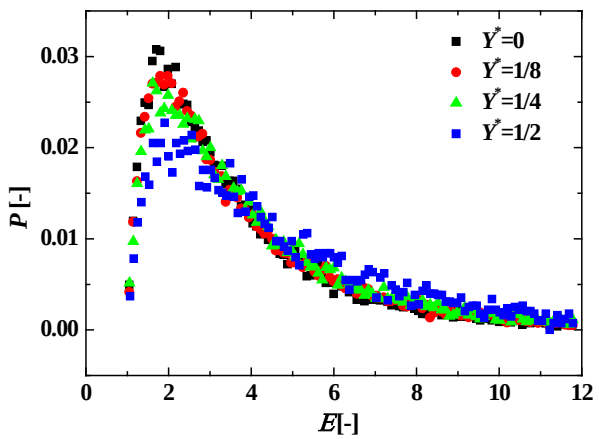

Figure 10. Probability density distribution of the roundness of dye patches for the case of wall-bounded shear flow: different Y^* for $X^* = 30$.

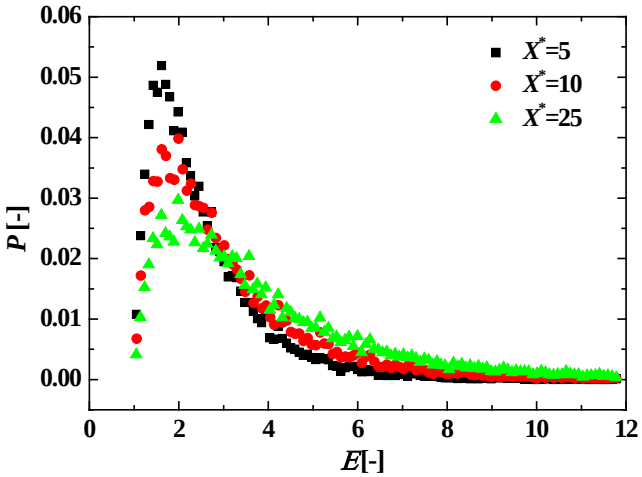

(a)

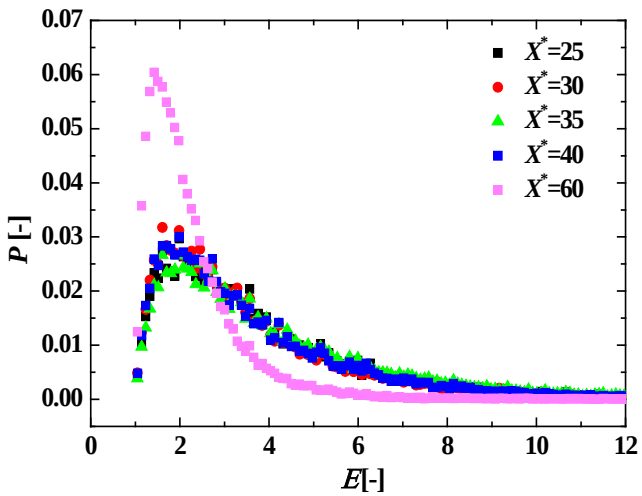

(b)

Figure 11. Same as **Figure 10**, but for the case of homogeneous flow case: to see clearly, the results of seven observation sites are separated into two sub-figures. (a) X^* = 5, 10 and 25; (b) X^* = 25, 30, 35, 40 and 60.

the two figures, it also can be confirmed that the roundness always has values larger than 1, and for both cases, the value tend to be around 1.5 to 2.5. That is to say, compared with circle shapes, the dye patch are always stretched to some extent, even in the case when the shear effect is absent. It is inferred that shear effect is not the only reason for the slim dye shape. In the homogeneous flow and away from the wall in the shear flow, the larger integral length scale in the streamwise direction over the spanwise direction also has an influence.

6. Conclusions

In this study, the effect of dye injection location on the dye patches is investigated by releasing dye solution into a wall-bounded shear flow at different wall-normal distances

from the wall. Moreover, the effect of streamwise diffusion distance on the development of dye patch distribution is studied. The dye plume images are recorded with a PLIF technique. Based on image processing, the high-intensity dye patches are extracted from the PLIF images. Then, the orientation angle and the roundness of each dye patch are calculated and analyzed statistically.

We found that the high-intensity dye patches have larger probability of being positively orientated when the shear effect at the injection location is strong, much different from the equal probability of being negative and positive in the homogeneous cases. An increasing asymmetry is observed when the injection location is far away from the wall. The roundness distribution indicates that the dye patches are always stretched to some extent, due to the shear effect and the different integral length scale in the streamwise and spanwise directions. Also from the results, the probability density function of neither the orientation angle nor the roundness depends on the streamwise diffusion distance in the wall-bounded shear flow.

Acknowledgements

Thanks to the following: 1) Open Journal of Fluid Dynamics for publishing this paper; 2) Daichi Sekine, Yonghai Zhang, Masaya Endo and Yuji Sato for their cooperation with PLIF measurement and programming.

References

[1] Taylor, G.I. (1921) Diffusion by Continuous Movement. *Proceedings of the Royal Society A*, **20**, 196-211.

[2] Richardson, L.F. (1926) Atmospheric Diffusion Shown on a Distance-Neighbor Graph. *Proceedings of the Royal Society A*, **110**, 709-737. https://doi.org/10.1098/rspa.1926.0043

[3] Lakshmi, P.D. (2000) Statistical Characteristics of Turbulent Chemical Plumes. Ph.D. Dissertation, Georgia Institute of Technology, Georgia.

[4] Webster, D.R., Roberts, P.J.W. and Raad, L. (2001) Simultaneous DPTV/PLIF Measurements of a Turbulent Jet. *Experiments in Fluids*, **30**, 65-72. https://doi.org/10.1007/s003480000137

[5] Crimaldi, J.P. and Koseff, J.R. (2001) High-Resolution Measurements of the Spatial and Temporal Scalar Structure of a Turbulent Plume. *Experiments in Fluids*, **31**, 90-102. https://doi.org/10.1007/s003480000263

[6] Webster, D.R, Rahman, S. and Dasi. L.P. (2001) On the Usefulness of Bilateral Comparison to Tracking Turbulent Chemical Odor Plumes. *Limnology and Oceanography*, **46**, 1048-1053. https://doi.org/10.4319/lo.2001.46.5.1048

[7] Tsukahara, T., Oyagi, K. and Kawaguchi, Y. (2016) Estimation Method to Identify Scalar Point Source in Turbulent Flow based on Taylor's Diffusion Theory. *Environment Fluid Mechanics*, **16**, 521-537. https://doi.org/10.1007/s10652-015-9436-x

[8] Moore, P.A. and Atema, J. (1991) Spatial Information in the Three-Dimensional Fine Structure of an Aquatic Odor Plume. *The Biological Bulletin*, **181**, 408-418. https://doi.org/10.2307/1542361

[9] Webster, D.R. and Weissburg, M.J. (2001) Chemosensory Guidance Cues in a Turbulent Chemical Odor Plume. *Limnology and Oceanography*, **46**, 1034-1047.

https://doi.org/10.4319/lo.2001.46.5.1034

[10] Page, J.L., Dickman, B.D. Webster, D.R. and Weissburg, M.J. (2011) Getting Ahead: Context-Dependent Responses to Odor Filaments Drives Along-Stream Progress during Odor Tracking in Blue Crabs. *Journal of Experiment Biology*, **214**, 1498-1512. https://doi.org/10.1242/jeb.049312

[11] Endo, M., Tsukahara, T. and Kawaguchi, Y. (2015) Relationship between Diffusing-Material Lumps and Organized Structures in Turbulent Flow. *Proceedings of the* 5*th International AJK Joint Fluids Engineering Conference*, Seoul, 26-31 July 2015, 1747-1753.

[12] Crimaldi, J.P., Wiley, M.B. and Koseff, J.R. (2002) The Relationship Between Mean and Instantaneous Structure in Turbulent Passive Scalar Plumes. *Journal of Turbulence*, **3**, 1-24.

[13] Fackrell, J.E. and Robins, A.G. (1982) Concentration Fluctuations and Fluxes in Plumes from Point Source in a Turbulent Boundary Layer. *Journal of Fluid Mechanics*, **117**, 1-26. https://doi.org/10.1017/S0022112082001499

[14] Otsu, N. (1979) A Threshold Selection Method from Gray-Level Histograms. *IEEE Transactions on Systems*, *Man*, *and Cybernetics*, **9**, 62-66. https://doi.org/10.1109/TSMC.1979.4310076

[15] Liao, P.S., Chen, T.S. and Chung, P.C. (2001) A Fast Algorithm for Multilevel Thresholding. *Journal of Information Science and Engineering*, **17**, 713-727.

[16] He, L., Chao, Y., Suzuki, K. and Wu, K. (2009) Fast Connected-Component Labeling. *Pattern Recognition*, **42**, 1977-1987. https://doi.org/10.1016/j.patcog.2008.10.013